Science of the Total Environment 544 (2016) 722–729

Contents lists available at ScienceDirect

Science of the Total Environment

journal homepage: www.elsevier.com/locate/scitotenv

Short and long term biosorption of silica-coated iron oxide nanoparticles in heterotrophic biofilms

Maria P. Herrling [a], Susanne Lackner [a,b], Oleg Tatti [a], Gisela Guthausen [c], Markus Delay [a], Matthias Franzreb [d], Harald Horn [a,e,*]

[a] Engler-Bunte-Institut, Chair of Water Chemistry and Water Technology, Karlsruhe Institute of Technology (KIT), Engler-Bunte-Ring 1, 76131 Karlsruhe, Germany
[b] Urban Bioengineering for Resource Recovery, Bauhaus-Institute for Infrastructure Solutions, Bauhaus-Universität Weimar, Coudraystraße 7, 99423 Weimar, Germany
[c] Pro²NMR, Institute for Biological Interfaces 4 and Institute for Mechanical Process Engineering and Mechanics, Karlsruhe Institute of Technology, Adenauerring 20b, 76131 Karlsruhe, Germany
[d] Institute of Functional Interfaces, Karlsruhe Institute of Technology (KIT), Hermann-von-Helmholtz-Platz 1, 76344 Eggenstein-Leopoldshafen, Germany
[e] DVGW Research Laboratories for Water Chemistry and Water Technology, Engler-Bunte-Ring 1, 76131 Karlsruhe, Germany

HIGHLIGHTS

- $scFe_3O_4$-NP mainly attach to the outer biofilm layers and biofilm detachment occurs.
- Biosorption of $scFe_3O_4$-NP onto biofilms happens quickly, but is rather low.
- Transport of $scFe_3O_4$-NP in the liquid is more dominant than sorption to biofilms.
- 57% of input $scFe_3O_4$-NP exits the MBBR, indicating low retention capacity.

GRAPHICAL ABSTRACT

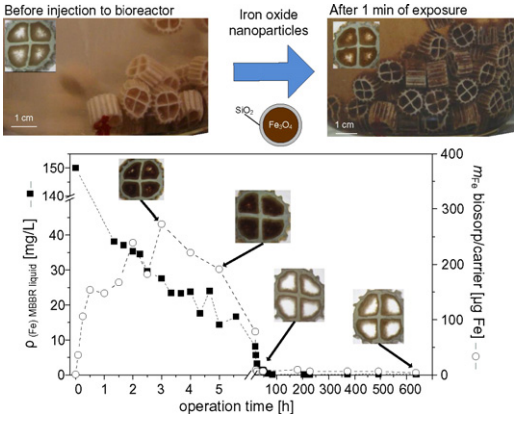

ARTICLE INFO

Article history:
Received 10 October 2015
Received in revised form 29 November 2015
Accepted 30 November 2015
Available online 10 December 2015

Editor: D. Barcelo

Keywords:
Magnetic nanoparticles
Wastewater treatment
Magnetic susceptibility

ABSTRACT

The increased application of engineered nanoparticles (ENP) in industrial processes and consumer products has raised concerns about their impact on health and environmental safety. When ENP enter the global water cycle by e.g. wastewater streams, wastewater treatment plants (WWTP) represent potential sinks for ENP. During biological WWT, the attachment of ENP to biofilms is responsible for the desired removal of ENP from the water phase avoiding their release into the aquatic environment. However, the fundamental mechanisms guiding the interactions between ENP and biofilms are not yet fully understood. Therefore, this study investigates the behavior and biosorption of inorganic ENP, here magnetic iron oxide nanoparticles coated with silica ($scFe_3O_4$-NP), with heterotrophic biofilms at different time scales. Their magnetic properties enable to follow $scFe_3O_4$-NP in the biofilm system by a magnetic susceptibility balance and magnetic resonance imaging. Biofilms were exposed to $scFe_3O_4$-NP at short contact times (5 min) in flow cells and complementary, $scFe_3O_4$-NP were introduced into a moving bed biofilm reactor (MBBR) to be observed for 27 d. Mass balances revealed that $scFe_3O_4$-NP sorbed to the biofilm within a few minutes, but that the total biosorption was rather low (3.2 µg Fe/mg TSS). $scFe_3O_4$-NP

* Corresponding author: Engler-Bunte-Institut, Chair of Water Chemistry and Water Technology, Karlsruhe Institute of Technology (KIT), Engler-Bunte-Ring 9, 76131 Karlsruhe, Germany.
E-mail address: harald.horn@kit.edu (H. Horn).

http://dx.doi.org/10.1016/j.scitotenv.2015.11.174

Biomass
Mass balance

mainly sorbed to the biofilm surface inducing the detachment of outer biofilm parts starting after an exposure time of 3 h in the MBBR. The biosorption depended on the exposure concentration of $scFe_3O_4$-NP, but less on the contact time. Most $scFe_3O_4$-NP exited the flow cell (up to 65%) and the MBBR (57%) via the effluent. This effect was favored by the stabilization of $scFe_3O_4$-NP in the bulk liquid by organic matter leading to a low retention capacity of the MBBR system. The results contribute to improve our understanding about the fate of ENP in environmental and in technical biofilm systems and give indications for future investigations needed.

1. Introduction

The increasing application of products implementing nanotechnology contributes to the release of engineered nanoparticles (ENP) into the aquatic environment (Delay and Frimmel, 2012; Gottschalk and Nowack, 2011; Klaine et al., 2008). The distribution and fate of ENP in the environment has been the focus of many experimental and modeling studies to evaluate potential negative impacts on ecosystems and human health (Gottschalk et al., 2013a; Schaumann et al., 2015; Sun et al., 2014). With respect to the distribution of ENP in the environment, their interactions with biofilms have a major impact on mass flows and bioavailability (Fabrega et al., 2011; Westerhoff et al., 2013). As in most environments microorganisms preferentially exist in form of biofilms, a fundamental understanding of the interactions of ENP with biofilms is critical to understand the fate of ENP in environmental and technical systems (Ikuma et al., 2015). When ENP enter the water cycle by e.g. wastewater streams, ENP will potentially end up in wastewater treatment plants (WWTP) which represent sinks for ENP. Therefore, it is crucial to investigate the behavior of ENP in WWTP, not least for reasons of pollution control. The biological treatment step, in particular, contributes to the removal of ENP from the wastewater (WW) through interactions of ENP with the biomass, such as attachment by sorption processes (Brar et al., 2010; Kiser et al., 2010). Estimated concentrations of various ENP in WWTP effluents are in the concentration range of a few ng/L to 5 μg/L as summarized in Gottschalk et al. (2013b). For example, measured concentrations were reported to be <12 ng/L for Ag-NP (Li et al., 2013) and <5 to 15 μg/L for TiO_2-NP (Kiser et al., 2009). Compared to conventional activated sludge systems, technical systems employing biofilms, such as moving bed biofilm reactors (MBBR), in which biofilms are attached to plastic carrier materials (McQuarrie and Boltz, 2011; Odegaard et al., 1994; Wessman et al., 2004) are an only little investigated regarding their removal of ENP. Recent studies show that the removal of various ENP during WWT is influenced by a complex framework of parameters, i.e. biofilm properties (e.g. biofilm compactness) (Gu et al., 2014), particle properties (e.g. particle size and surface properties) (Peulen and Wilkinson, 2011) and water matrix (Battin et al., 2009; Fabrega et al., 2011). Furthermore, the experimental setup as the type of bioreactor (e.g. batch experiments (Kaegi et al., 2013; Rottman et al., 2012), sequencing batch reactors (Wang et al., 2012; Yang et al., 2015), membrane bioreactors (Tan et al., 2015) or pilot WWTP (Hou et al., 2013; Kaegi et al., 2011)) plays a key role. This leads to a high variability of the removal efficiency for different kinds of ENP in WWT, which can between 10 and 90% in laboratory scale up to field-scale systems (Westerhoff et al., 2013). So far, the term "biosorption" is commonly used in WWT to summarize the total chemical and physical sorption mechanisms of ENP to the biomass by sorption to the cells and extra cellular polymeric substances (EPS) as well as bio-uptake (Kiser et al., 2010). In this context, it has recently been stated that biofilms generally serve as efficient "sponges" for ENP, but efforts to elucidate the fundamental mechanisms driving the interactions of ENP and biofilms are still at an early stage (Ikuma et al., 2015). Especially for newer WWT technologies employing biofilms, such as MBBR systems, research is needed to evaluate if the mentioned "sponge-like" behavior for ENP can be transferred to all biofilms. Information gained about the sorption of ENP to the biofilm is relevant to estimate their mass flows in the aquatic environment in short and long term. To the authors' knowledge, there is no study about the fate of ENP in MBBR based biofilm systems under complex hydrodynamic conditions. The behavior of ENP entering MBBR systems is still uncertain and needs to be investigated to evaluate the MBBR's risk potential for the release of ENP at different time scales.

To meet this gap, the pathways and interactions of silica-coated iron oxide nanoparticles ($scFe_3O_4$-NP) with biofilms in MBBR systems were assessed. $scFe_3O_4$-NP (particle core made of Fe_3O_4) were utilized as tracer nanoparticle. Their magnetic properties enable their sensitive quantification via a magnetic susceptibility balance and their in-situ and *non-invasive* visualization within the biofilm matrix using magnetic resonance imaging (MRI). The experimental approach has been demonstrated and evaluated in a previous study (Herrling et al., 2015a).

The main goals of this work were to:

(1) Investigate the biosorption of $scFe_3O_4$-NP onto biofilm carriers in flow cell experiments at short contact times.
(2) Asses the removal and behavior of $scFe_3O_4$-NP during continuous MBBR operation.
(3) Establish mass balances for $scFe_3O_4$-NP to get insights into the time and concentration dependent biosorption onto the biofilm.
(4) Visualize the biosorption of $scFe_3O_4$-NP within the biofilm matrix using MRI.

2. Materials and methods

2.1. MBBR operation and biofilm characterization

A laboratory scale MBBR (V_{MBBR} = 700 ml) filled with K1 polyethylene carrier material (diameter: 9 mm, AnoxKaldnes AB, Sweden) with a filling ratio of 25% using 110 plastic carriers was operated for 6 months (Fig. 1 A). The cylindrical carrier material (Fig. 1B) had a specific surface area of 500 m^2/m^3. The reactor was fed with acetate for the cultivation of heterotrophic biofilms (substrate composition in Supporting information Table SI 1). The hydraulic retention time (HTR) for the cultivation of the biofilm (3 months) was set to 15 h to minimize washout of the bacteria and was then stepwise reduced to 5 h for the $scFe_3O_4$-NP exposure experiments. Thorough mixing and oxygen saturation was guaranteed by aeration with pressurized air. The pH value was set to 8–9 by dosing acidic water (0.014% HCl solution). The electrical conductivity (~1500 μS/cm) remained stable over the whole experiment. During the reactor operation, the soluble chemical oxygen demand (COD, filtered with 0.45 μm filter) was monitored using tests kits (LCK 414, HACH LANGE GmbH, Düsseldorf, Germany). The amount of biomass attached to the carriers was quantified by determining the total suspended solid content (TSS) using 5 carriers. Biofilms were imaged using a stereomicroscope (Stereomicroscope SMT, Rathenow, Germany).

2.2. $scFe_3O_4$-NP: preparation and characterization

Silica coated iron oxide nanoparticles ($scFe_3O_4$-NP) (MagPrep25 silica magnetic nanoparticles, ρ_{stock}(Fe) = 35 g/L, Merck KGaA, Darmstadt, Germany) with a primary particle size of 25 nm were used. $scFe_3O_4$-NP consisted of a magnetite core (Fe_3O_4) and a silica shell (SiO_2) which

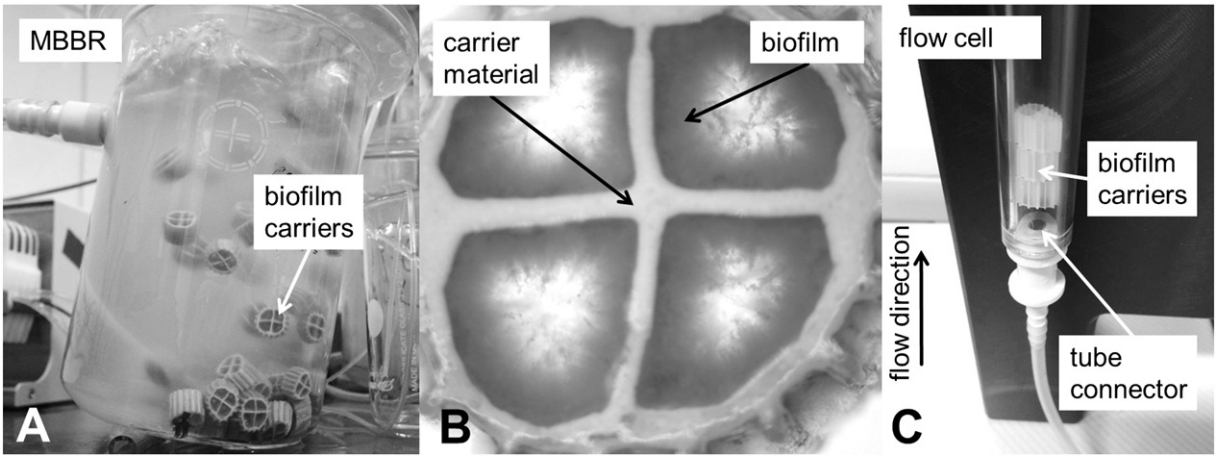

Fig. 1. A) Continuous MBBR with biofilm carriers mixed by aeration (no addition of $scFe_3O_4$-NP). B) Heterotrophic biofilm cultivated on a plastic carrier (K1, AnoxKaldnes, Sweden). C) Experimental setup for the flow cell experiments where biofilm carriers were exposed to different concentrations of $scFe_3O_4$-NP while the HRT was kept constant (flow direction from bottom to top as indicated by the arrow).

prevented oxidation or release of iron ions. The core and the shell were expected to be stable over the whole experiment due to the low water-solubility of the used $scFe_3O_4$-NP at pH values >3 in aqueous solution at room temperature (Nirschl, 2014). $scFe_3O_4$-NP were selected due to their magnetic property which enables a new analytical approach to assess their fate in biofilm systems (quantification via magnetic susceptibility and their visualization via magnetic resonance imaging).

Prior to the experiments, suspensions of $scFe_3O_4$-NP were diluted in ultrapure water (Milli-Q, Merck Millipore, Billerica, Massachusetts, USA), mechanically mixed, treated in ultrasonic bath (1 h) and settled for 20 h. Then, the stable decanted supernatant was diluted to the desired concentration of $scFe_3O_4$-NP (ρ(Fe) = 200; 400; 1000 mg/L). The applied concentrations of $scFe_3O_4$-NP in the experiments were chosen to be higher than the expected environmental concentrations for nanomaterials (Gottschalk et al., 2013b). Concentrations of up to 1000 mg/L Fe were used to better identify the driving forces and the distribution of $scFe_3O_4$-NP. However, the behavior of $scFe_3O_4$-NP at lower concentrations might be different. The concentration of $scFe_3O_4$-NP in the liquid phase and biosorbed to the biofilms was determined based on their magnetic property using a magnetic susceptibility balance (MSB) for magnetic susceptibility measurement (χ) (Sherwood Scientific, Cambridge, England, detection limit of $\chi_{V\,\mathrm{min}} = 0.001 \cdot 10^{-7}$ provided by the manufacturer). This approach has been demonstrated in a previous study (Herrling et al., 2015a). To calculate the concentration of $scFe_3O_4$-NP, their magnetic susceptibility was correlated with their iron concentration (calibration curve in Supporting information Fig. SI 1), determined by inductively coupled plasma optical emission spectrometry (ICP-OES, Varian Vista Pro, Agilent Technologies, Santa Clara, USA; calibration limit for Fe: 10 μg/L; after *aqua regia* digestion). For further information about the theory and precision of the magnetic susceptibility, please refer to Supporting information Section 1 and to a previously conducted study (Herrling et al., 2015a).

For the basic characterization of $scFe_3O_4$-NP, the particle size (hydrodynamic diameter) was determined by dynamic light scattering and laser Doppler anemometry (Zetasizer Nano ZS, Malvern Instruments GmbH, Herrenberg, Germany). For the measurement, the refraction index (RI) and absorption (Abs.) for iron oxide were used: RI = 2.420, Abs. = 0.010. Furthermore, the zeta potential was measured with a combination of laser Doppler electrophoresis and phase analysis light scattering (M3-PALS), applying the Smoluchowski equation with the same device. The measurements were performed in ultrapure water, because the matrix effects of the substrate disturbed the measurement. $scFe_3O_4$-NP had a particle size of 87 ± 20 nm (at ρ(Fe) = 4.4 mg/L), indicating that they tend to form agglomerates (primary particle size of MagPrep25 silica magnetic nanoparticles was 25 nm). The point of zero charge (ρ(Fe) = 4.4 mg/L) was between a pH value of 5–6 (see Supporting information Fig. SI 2). In the relevant pH range for the MBBR operation (pH value 8–9), $scFe_3O_4$-NP had a zeta potential of ~− 20 mV.

2.3. Flow cell experiment and mass balance

Short term exposure experiments were conducted using a transparent plastic tube serving as flow cell (FC) (V_{FC} was 7.8 mL to10.7 mL depending on the number of inserted carriers ($n_{\mathrm{blank\ carrier}}$ and $n_{\mathrm{biofilm\ carrier}}$)). The FC was connected to a peristaltic pump (REGLO Digital MS-4/12, ISMATEC, Germany), see experimental setup in Fig. 1C. The desired number of carriers was placed into the FC directly at the bottom inlet. The inner crosses of the carriers were aligned to reduce flow resistance. Prior to the experiments, the FC system was pre-conditioned with

Table 1
Summary of flow cell (FC) experiments with varying number of blank ($n_{\mathrm{blank\ carrier}}$) and of biofilm carriers ($n_{\mathrm{biofilm\ carrier}}$). All experiments were conducted in triplicates (except tube-1000 and 3bio-400 (duplicates)). $\rho_{\mathrm{pulse\ injection}}$(Fe) is the concentration of the pulse injection of $scFe_3O_4$-NP and $m_{\mathrm{Fe\ entry\ FC}}$ corresponds to the total iron mass of the pulse. ρ_{FC}(Fe) is the calculated exposure concentration in the flow cell and $m_{\mathrm{Fe\ loading\ FC}}$ represents calculated loading of $scFe_3O_4$-NP per carrier assuming that all $scFe_3O_4$-NP ($m_{\mathrm{Fe\ entry\ FC}}$) sorb homogenously to all biofilm carriers.

Experiment	$n_{\mathrm{blank\ carrier}}$ –	$n_{\mathrm{biofilm\ carrier}}$ –	$\rho_{\mathrm{pulse\ injection}}$(Fe) [mg/L]	$m_{\mathrm{Fe\ entry\ FC}}$ [μg]	ρ_{FC}(Fe) [mg/L]	$m_{\mathrm{Fe\ loading\ FC}}$ [μg/carrier]
Tube-1000	–	–	1000	946	88	–
10blank-1000	10	–	1000	946	105	–
10bio-1000	–	10	1000	946	123	95
3bio-1000	7	3	1000	1080	138	360
3bio-400	7	3	400	381	49	127
3bio-200	7	3	200	201	26	67

a suspension of $scFe_3O_4$-NP (ρ(Fe) = 1000 mg/L) which was recirculated for 2 h. The experimental series were conducted in triplicates (except tube-1000 and 3bio-400 (duplicates)) varying the number of biofilm carriers and the injection concentration ($\rho_{\text{pulse injection}}$(Fe), $V_{\text{injection FC}} = 1$ mL), see Table 1.

For the experiments, demineralized water was pumped through the system with flow velocities of 1.7–2.3 mm/s without recirculation (from bottom to top). The HRT was kept constant (~1.3 min). To start the experiment suspensions of $scFe_3O_4$-NP ($\rho_{\text{pulse injection}}$(Fe) = 200; 400; 1000 mg/L) were injected once as a pulse into the system and the demineralized water was continuously pumped through as eluent. The $scFe_3O_4$-NP in the total eluent were manually collected by sampling vessels and measured offline via MSB ($n = 3$). At the end of each flow cell experiment (~5 min of perfusion until detection of pure water as eluent) a mass balance for $scFe_3O_4$-NP was established according to Eq. (1).

$$m_{\text{Fe entry FC}} = m_{\text{Fe outlet FC}} + m_{\text{Fe sediment FC}} + m_{\text{Fe biosorp FC}} + m_{\text{Fe losses FC}} \quad (1)$$

The total mass of iron injected to the FC system ($m_{\text{Fe entry FC}}$) equals: the $scFe_3O_4$-NP passing the FC ($m_{\text{Fe outlet FC}}$), plus the $scFe_3O_4$-NP which settled during the experiment ($m_{\text{Fe sediment FC}}$) on the tube connector (see indication in Fig. 1C), plus the portion of $scFe_3O_4$-NP which sorbed to the biofilm ($m_{\text{Fe biosorp FC}}$). Within this study, the term biosorption is used as the sum of all sorption processes of $scFe_3O_4$-NP (chemical and physical sorption processes and bio uptake) to the biofilms according to Kiser et al. (2010). The losses described by $m_{\text{Fe losses FC}}$ attribute to the experimental procedure or due to loosing $scFe_3O_4$-NP by opening-up the flow cell system. The used $scFe_3O_4$-NP were expected to be chemically stable under the experimental conditions and the short experimental time (5 min). Therefore, losses caused by dissolution of the $scFe_3O_4$-NP are neglected.

2.4. MBBR experiment and mass balance

A continuous flow experiment was conducted using a MBBR to investigate the effect of the real water matrix on the fate and biosorption of $scFe_3O_4$-NP in long term (Table 2). The original reactor medium was sieved to remove particulate matter (13.6 μm precision sieve) and was further used as water matrix for the experiment. The exposure concentration (ρ_{MBBR}(Fe)) was in the same concentration range as the ones used for the short term flow cell experiments (ρ_{FC}(Fe)). The loading of $scFe_3O_4$-NP per carrier ($m_{\text{Fe loading MBBR}}$), assuming that all $scFe_3O_4$-NP sorb homogenously to all biofilm carriers in the MBBR (without reaching saturation) was 3–14 times higher than for the flow cell experiments (compare Tables 1 and 2). This was defined due to the increased complexity of the system (MBBR), where more uncertainties and losses for the recovery of $scFe_3O_4$-NP are expected. To start the MBBR experiment, the stock solution of $scFe_3O_4$-NP ($\rho_{\text{injection MBBR}}$(Fe) = 35 g/L) of $V_{\text{injection MBBR}} = 3$ mL was directly added into the MBBR (main reactor vessel) while aeration was on to ensure thorough mixing. $scFe_3O_4$-NP were injected only once. During the MBBR experiment samples were taken (5 mL) positioning a conventional syringe 6 cm below the water surface of the MBBR after 5 min settling time (no aeration). Samples from the MBBR liquid were taken every 15 min starting from 80 min and from 4 h each hour and starting from 20 h once per day for 27 days to study the long term fate of $scFe_3O_4$-NP in the MBBR. The concentration of $scFe_3O_4$-NP was measured manually by the MSB ($n = 3$), as described in the Supporting information Section 1.2. Biofilm carriers were imaged using a stereomicroscope upfront to the magnetic susceptibility measurement. To trace the distribution of the $scFe_3O_4$-NP a mass balance was established over the operation period of 0–5 h, 0–18 h and 0–27 h according to Eq. (2).

$$m_{\text{Fe entry MBBR}} = m_{\text{Fe outlet MBBR}} + m_{\text{Fe liquid MBBR}} + m_{\text{Fe biosorp MBBR}} \times n_{\text{biofilm carrier}} + m_{\text{Fe sampling MBBR}} + m_{\text{Fe losses MBBR}} \quad (2)$$

The initially injected $scFe_3O_4$-NP ($m_{\text{Fe entry MBBR}}$) can be described as the sum of $scFe_3O_4$-NP leaving the MBBR via the outlet ($m_{\text{Fe outlet MBBR}}$), plus the $scFe_3O_4$-NP still being in the liquid of the MBBR ($m_{\text{Fe liquid MBBR}}$), plus $scFe_3O_4$-NP which sorb to the biofilm carriers ($m_{\text{Fe biosorp MBBR}}$ times the number of biofilm carriers ($n_{\text{biofilm carrier}}$)), and plus the $scFe_3O_4$-NP which were removed from the MBBR by the sampling routine ($m_{\text{Fe sampling MBBR}}$). The $scFe_3O_4$-NP which could not be recovered during the experiment is summarized in the term $m_{\text{Fe losses MBBR}}$. The used $scFe_3O_4$-NP were expected to be chemically stable under the moderate experimental conditions (neutral pH), therefore, losses caused by dissolution of the $scFe_3O_4$-NP have been neglected.

2.5. Magnetic resonance imaging methods

To support the quantitative results obtained by MSB, biofilm carriers were imaged using magnetic resonance imaging (MRI) for *non-invasive* visualization of the biosorption of $scFe_3O_4$-NP in the biofilm matrix. Prior to MRI, the carriers where shaken overhead (30 rpm, for 12 h) in suspensions of $scFe_3O_4$-NP ($V = 30$ mL) of ρ(Fe) = 90 mg/L and ρ(Fe) = 350 mg/L given the same exposure concentration range as in the flow cell and MBBR experiments. $scFe_3O_4$-NP serve as contrast agents in MRI. The influence of $scFe_3O_4$-NP on the relaxation properties (T_1 relaxation) of ^{1}H nuclei (mainly in water molecules) in the biofilm was investigated using a high-field (200 MHz) MRI tomograph (Bruker Avance 200 SWB, Bruker BioSpin GmbH, Rheinstetten, Germany). The assessment of the distribution of various iron oxide nanoparticles in porous media (quartz sand) using MRI has been demonstrated in a previous study (Cuny et al., 2015). The single carriers were placed into the tomograph with tap water as surrounding liquid using an in-house sample holder. The superconducting magnet had a magnetic-flux density B_0 of 4.7 T and a 150 mm vertical bore. The Bruker gradient system micro2.5 was used with a ^{1} H-NMR bird-cage (25 mm inner diameter). The images were taken applying a modified multi-slice multi-echo sequence (MSME). For information on the acquisition parameter and basics about MRI of $scFe_3O_4$-NP, please see Supporting information (Table SI 3 and Section 3). Principles of MRI are given in textbooks (Callaghan, 1991; Kimmich, 1997).

3. Results and discussion

3.1. Flow cell experiments: biosorption of $scFe_3O_4$-NP at short contact times

To investigate the behavior of $scFe_3O_4$-NP in a simplified experimental environment, series of flow cell experiments were performed using demineralized water as eluent (Table 1). The heterotrophic biofilms used were light brownish and exhibited fluffy and open structures (see Fig. 1B). Despite the fluffy physical structure, no detachment of biofilm parts could be observed in the flow cell experiments, in which biofilms were exposed to $scFe_3O_4$-NP for a short time period. Fig. 2A presents the mass balance of the normalized Fe mass ($m_{\text{Fe norm}}$) for the flow cell experiments according to Eq. (1) with a good mass balance closure of 4–30%. The amount of biofilm in one single carrier was stable (86 ± 5 mg TSS/carrier ($n = 5$)) contributing to low variability of the

Table 2
The MBBR ($V_{\text{MBBR}} = 700$ mL) was operated with 110 biofilm carriers ($n_{\text{biofilm carrier}}$) at a HRT of 5 h (inlet 130–160 mL/h). The iron mass injected to the MBBR was $m_{\text{Fe entry MBBR}} = 100$ mg. ρ_{MBBR}(Fe) is the calculated exposure concentration and $m_{\text{Fe loading MBBR}}$ is the loading of $scFe_3O_4$-NP per carrier in the MBBR assuming that all $scFe_3O_4$-NP ($m_{\text{Fe entry MBBR}}$) homogenously sorb to all biofilm carriers.

Experiment	$n_{\text{biofilm carrier}}$ –	$m_{\text{Fe entry MBBR}}$ [mg]	ρ_{MBBR} (Fe) [mg/L]	$m_{\text{Fe loading MBBR}}$ [μg/carrier]
MBBR	110	100	150	940

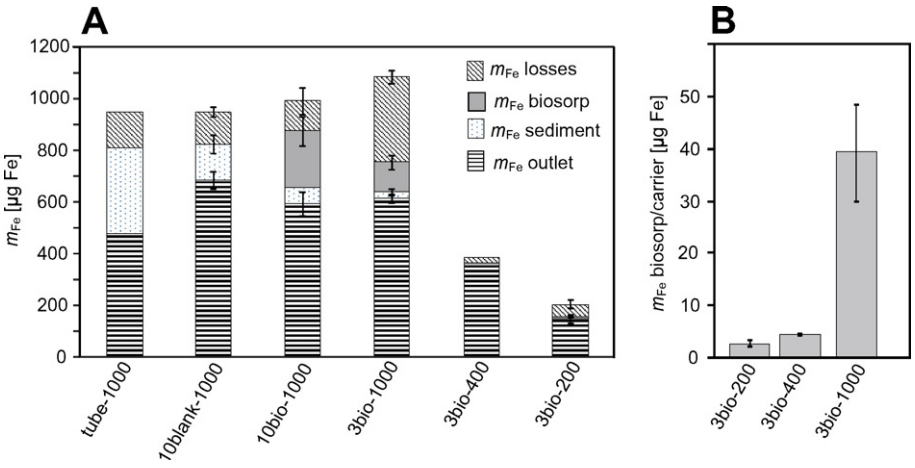

Fig. 2. A) Mass balance for m_{Fe} of flow cell (FC) experiments (see Table 1). The experiments were conducted in triplicates (except: tube-1000 and 3bio-400 (duplicates)). Here, $m_{Fe\ outlet}$ defines the $scFe_3O_4$-NP passing the flow cell with the eluent, $m_{Fe\ sediment}$ are the settled $scFe_3O_4$-NP during the flow cell experiment and $m_{Fe\ biosorp}$ represents $scFe_3O_4$-NP which sorbed on all inserted biofilm carriers. The portion of $m_{Fe\ losses}$ (4–30%) indicates that a reliable mass balance closure is achieved. B) Biosorption per carrier in experiments with 3 biofilm carriers and varying concentrations of $scFe_3O_4$-NP.

data. A positive effect of the blank carrier material on the stability of $scFe_3O_4$-NP is highlighted by the comparison of the empty flow cell (tube-1000) and the flow cell assembled with 10 blank carriers (10blank-1000). The lower retention of $scFe_3O_4$-NP in the flow cell filled with blank carriers compared to the one without carrier materials, is shown by less sedimentation ($m_{Fe\ sediment}$) and a more efficient transport of $scFe_3O_4$-NP through the flow cell ($m_{Fe\ outlet}$).

The better mixing in the flow cell kept $scFe_3O_4$-NP in suspension. Comparing 10blank-1000 and 10bio-1000 the stabilizing effect of the presence of the heterotrophic biofilm on $scFe_3O_4$-NP was evident from the increased portion of $scFe_3O_4$-NP in the outlet and decreased portion of settled $scFe_3O_4$-NP. These results indicate that dissolved and particulate organic matter (OM) which was most likely released by the biofilm matrix (i.e. extracellular polymeric substances, EPS) significantly stabilized the $scFe_3O_4$-NP in the flow cell. This might be due to the coating of the particle surface of $scFe_3O_4$-NP with OM leading to their stabilization in the bulk liquid. A previous study showed that biomass from a WWTP releases OM, which stabilized PVA-coated $scFe_3O_4$-NP in the bulk liquid (Herrling et al., 2015a). OM is known for its ability to coat the surface of ENP, leading to steric as well as electrostatic stabilization in the bulk liquid (Delay et al., 2011; Zhang et al., 2009). The portion for $m_{Fe\ outlet}$ was high (up to 65% of input $scFe_3O_4$-NP) for all flow cell experiments indicating that the transport of $scFe_3O_4$-NP was favored. Furthermore, the mass balance gives evidence on the biosorption of $scFe_3O_4$-NP to biofilms ($m_{Fe\ biosorp}$). Generally spoken, electrostatic, steric and hydrophobic interactions of ENP with biofilms might take place, whereas, the attachment can mainly be attributed to sorption processes (chemisorption and physical sorption), as well as entrapment of $scFe_3O_4$-NP in the heterogeneous structures of the biofilm (Brar et al., 2010; Ikuma et al., 2015). In the presented mass balance, $m_{Fe\ biosorp}$ represents the total biosorption to the biofilm carriers used in the experiments (either 3 or 10). During all the experiments, no preferential biosorption was found on the biofilm carriers located at the entrance of the flow cell. By reducing the number of biofilm carriers (from 10 to 3) providing lower biofilm surface area (comparing 3bio-1000 and 10bio-1000) the total biosorption was reduced by 13% (Fig. 2A). Fig. 2 B shows the correlation between the pulse injection concentration of $scFe_3O_4$-NP and the biosorption per carrier for the flow cell experiments with 3 biofilm carriers. The positive correlation indicates that the biofilms might still provide free sorption sites and saturation has not been reached yet. Being aware of the limited data set, further experiments should focus on sorption rate experiments. In future investigations, lower concentration ranges of ENP should also be addressed to approach more realistic scenarios such as sewer systems or natural systems. However, the gained results demonstrate that the total biosorption per carrier was rather low compared to the input of $scFe_3O_4$-NP (see Table 1). $scFe_3O_4$-NP loadings of <5 µg Fe per carrier (for $m_{Fe\ entry\ FC} = 201$ and 381 µg Fe) and ~40 µg Fe per carrier (for $m_{Fe\ entry\ FC} = 1080$ µg Fe) were found. This highlights that transport of $scFe_3O_4$-NP in the surrounding bulk liquid is more dominant than the sorption to the biofilm in this case. Due to the measured particle size of $scFe_3O_4$-NP (~100 nm), cellular penetration and uptake can most likely be excluded (Peulen and Wilkinson, 2011). As the particle surface of ENP has a higher impact on the behavior in suspension than the core material (Lowry et al., 2012), the observed behavior in biofilm systems can be transferred to a certain extent to other ENP with comparable surface properties and sizes, such as the used $scFe_3O_4$-NP.

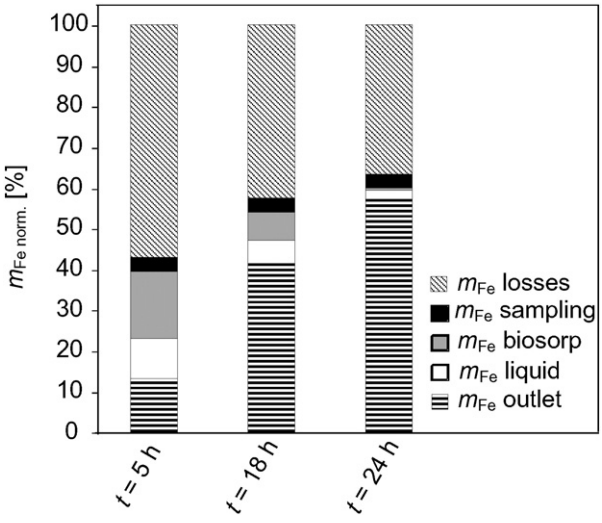

Fig. 3. Mass balance of the MBBR experiment after 5 h, 18 h and 24 h: $m_{Fe\ outlet}$ represents the portion of $scFe_3O_4$-NP, which exited the MBBR via outlet, $m_{Fe\ liquid}$ is the portion of $scFe_3O_4$-NP which was suspended in the MBBR bulk liquid, $m_{Fe\ biosorp}$ corresponds to $scFe_3O_4$-NP attached to biofilms, $m_{Fe\ sampling}$ represents the $scFe_3O_4$-NP which were removed by sampling and $m_{Fe\ losses}$ are the $scFe_3O_4$-NP which could not be recovered. $scFe_3O_4$-NP were determined using magnetic susceptibility ($n = 3$).

3.2. Behavior of scFe3O4-NP in MBBR: long term biosorption and mass balance

To investigate the behavior of $scFe_3O_4$-NP under more realistic conditions and in long term, a lab-scale MBBR experiment was performed over 27 days (Table 2). Here, complex hydraulic conditions due to the movement of the carriers (Herrling et al., 2015b) and a close to real waste water chemistry are expected to influence the fate of the $scFe_3O_4$-NP. The detailed distribution of $scFe_3O_4$-NP during MBBR operation is shown by a mass balance after 5 h, 18 h and 24 h after injection according to Eq. (2) (Fig. 3). From 24 h no change in the concentration of $scFe_3O_4$-NP and in the biosorption was detected. Therefore, the mass balance focuses on the specific time period between 0 h and 24 h.

The mass balance shows that $scFe_3O_4$-NP were mainly washed out of the MBBR instead of being retained in the biofilms by biosorption (Fig. 3). This finding confirms the low interaction between the $scFe_3O_4$-NP and the heterotrophic biofilms. Over an operation time of 5–24 h the portion of $scFe_3O_4$-NP released by the MBBR increased from 13 to 57% ($m_{Fe\ outlet\ MBBR}$) emphasizing the low retention capacity. This result is supported by the decrease of $scFe_3O_4$-NP in the liquid of the MBBR ($m_{Fe\ liquid\ MBBR}$). After 24 h, $scFe_3O_4$-NP were removed to 98% from the bulk liquid. However, the $scFe_3O_4$-NP removed from the bulk liquid did not necessarily end up completely sorbed onto the biofilms, but were transported out of the MBBR. The fraction of biosorption ($m_{Fe\ biosorp\ MBBR}$) decreased from 17% (after 5 h) to 0.5% (after 24 h) and most of the $scFe_3O_4$-NP exited the MBBR via the outlet. A negligible portion of the $scFe_3O_4$-NP was removed by sampling ($m_{Fe\ sampling\ MBBR}$) not affecting the mass balance result. The losses in the MBBR mass balance ($m_{Fe\ losses\ MBBR}$) are higher than in the flow cell experiments (Fig. 2), mainly due to the increased complexity of the system. However, after 24 h, 60% of $scFe_3O_4$-NP could be recovered and the temporal trend of the data gives insights into the fate of $scFe_3O_4$-NP in technical biofilm systems. This mass balance gap is slightly higher as the ones reported for other ENP in bioreactors for WWT (e.g. 18% balance gap, Gartiser et al., 2014).

To find answers for the extensive washout of $scFe_3O_4$-NP, a closer look on the biofilms during MBBR operation is necessary. Fig. 4 presents the temporal development of the concentration of $scFe_3O_4$-NP in the bulk liquid (squares) and the simultaneous biosorption of $scFe_3O_4$-NP per carrier (dots). Contrary to other studies with sampling intervals of several days (Wang et al., 2012), in this work samples were taken more frequently. The results reveal that $scFe_3O_4$-NP were removed from the bulk liquid very quickly within the first hour and were completely removed within 24 h (~6 times HRT). After 1 min contact time the biosorption in the MBBR reached ~40 μg Fe per carrier ($m_{Fe\ biosorp}$/carrier, Fig. 4), which is similar to the results of the flow cell experiment 3bio-100 (Fig. 2). This finding highlights that flow cell experiments can help to improve the understanding of the behavior of $scFe_3O_4$-NP in biofilm based bioreactors (e.g. MBBR) even though the hydrodynamic conditions are different. An unexpected trend occurred in the time resolved biosorption per carrier which could not be revealed by the mass balance. The biosorption first increased until 3 h of MBBR operation and decreased again reaching a low and stable level starting from 24 h up to 27 days ($m_{Fe\ biosorp}$ < 10 μg Fe per carrier). The

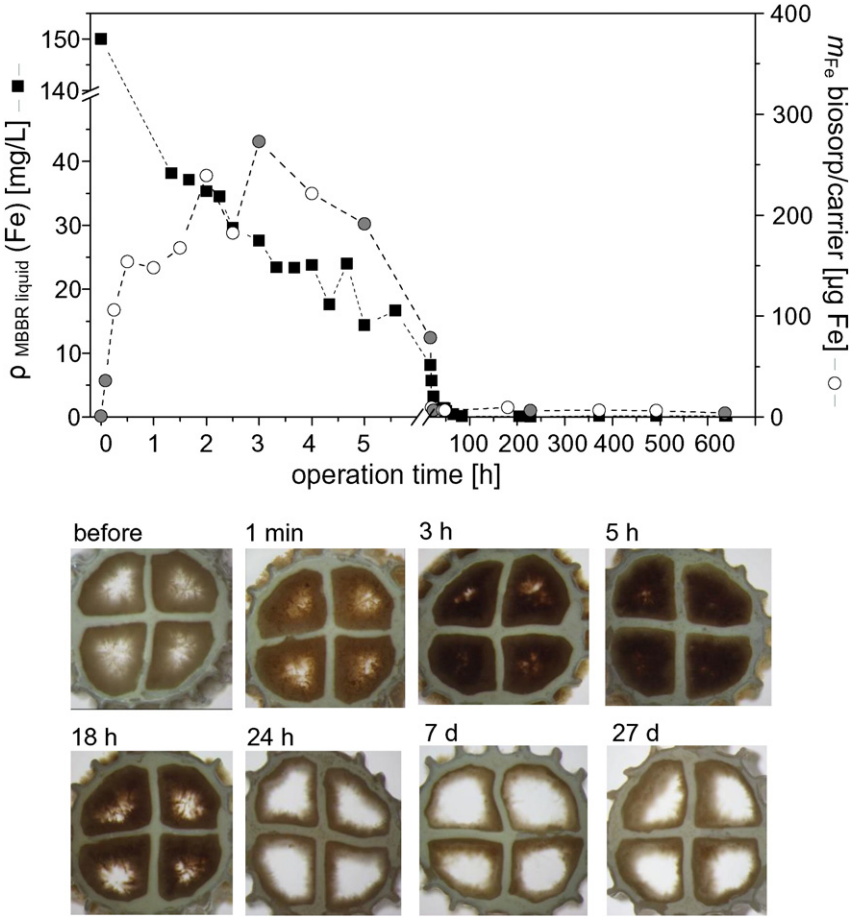

Fig. 4. Temporal development of the concentration of $scFe_3O_4$-NP in the bulk liquid (squares) and simultaneous biosorption per biofilm carrier (dots) during MBBR operation until 648 h (27 days). Please note that the *x*-axis (changing scale increments) and *y*-axis have breaks. Stereomicroscopic images below refer to gray indicated data points (dots) of the biosorption per carrier.

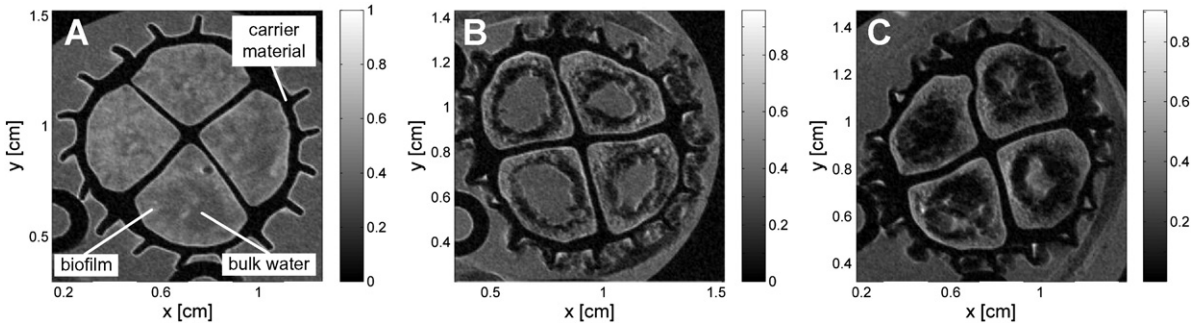

Fig. 5. MRI images of A) a blank biofilm carrier and biofilm carriers exposed to B) $scFe_3O_4$-NP of 90 mg/L Fe and C) 350 mg/L Fe. The spatial resolution is 59 μm..

maximum biosorption of $scFe_3O_4$-NP per carrier was 273 μg Fe corresponding to 3.2 μg Fe/mg TSS. Stereomicroscope pictures (Fig. 4) visualize the biosorption of $scFe_3O_4$-NP on and within the biofilm (becoming dark brownish). Biofilm parts loaded with $scFe_3O_4$-NP detached from the carrier material leading to a decrease of the measured biosorption per carrier starting from 3 h. Thereby, the biofilm thickness decreased. This strongly indicates that the heterotrophic biofilms are capable of retaining $scFe_3O_4$-NP only at short exposure times (up to 3 h) before $scFe_3O_4$-NP might be released by the detachment of loaded biofilm parts. Such a loss of biofilm parts might occur due to mechanical as well as metabolic stress. We assume that bacteria in the biofilm layers covered with $scFe_3O_4$-NP can be locally affected by lower substrate supply causing the biofilm structure to collapse and finally detach. Similar effects were found by Jing et al. (2014) where outer biofilm layers in monoculture biofilms were detached after exposure to CeO-NP as a self-protecting mechanism. However, the biological activity stayed stable during the MBBR experiment as monitored by the COD turnover (see Supporting information Fig. SI 3). The concentration of COD in the effluent remained constant which indicates no measurable toxic effects of the used $scFe_3O_4$-NP. This might be due to excess capacity of biomass in the used MBBR system which buffers the loss of biofilm. Furthermore, only outer biofilm layers might be affected by the $scFe_3O_4$-NP. Other nanomaterials, such as Ag-NP and TiO_2-NP, were also reported to have a low impact on the removal of COD in sequencing batch reactors (Wang et al., 2012). The measured biosorption in heterotrophic biofilms is in the same concentration range as those of recently published studies: In a sequencing batch reactor a maximum concentration of 10 μg Ag/mg TSS for Ag-NP (Yang et al., 2015), in a membrane bioreactor a maximum concentration of 28 μg Ag/mg MLSS (mixed liquor suspended solids) for Ag-NP (Yuan et al., 2015) and in full-scale WWTP concentrations of 1 to 6 μg Ti/mg TSS for TiO-NP (Kiser et al., 2009) were reported. However, in those studies, ENP were almost completely retained in the WWT system (up to 98% (Tan et al., 2015)) and no extensive washout was observed, as shown here for the MBBR. The low retention capacity of the MBBR for ENP might be attributed to its biomass in form of biofilms, which remove ENP less efficient compared to the commonly used activated sludge systems. This is due to the compact EPS structure of the biofilms. The compact EPS might hamper the interaction between ENP and the biofilm as demonstrated earlier using spherical biofilms (granular sludge) (Gu et al., 2014; Ma et al., 2013). This highlights the need to investigate different kinds of biomass from WWT for pollution control of ENP. The retention of ENP in those WWT systems will depend on the efficiency of post settling or other solid retention systems such as filtration as suggested by other studies (Wang et al., 2012; Westerhoff et al., 2013).

3.3. Visualization of the biosorption of $scFe_3O_4$-NP in biofilms

For the detailed visualization of the biosorption of $scFe_3O_4$-NP in the biofilm, MRI T_1-weighted images (spatial resolution of 59 μm) were taken after the exposure to different concentrations of $scFe_3O_4$-NP (ρ_0(Fe) = 0 mg/L, 90 mg/L and 350 mg/L), see Fig. 5A–C. MRI images give a deeper insight into the biosorption than stereoscopic images, which only proof the visible attachment at the outer side (Fig. 4).

In particular, the advantage of this imaging technique is the possibility of *non-invasive* and *in-situ* observations of wet biological samples compared to other destructive imaging methods such as electron microscopy, which is often applied to proof the sorption of nanomaterial onto biomass from WWT (Fabrega et al., 2009; Limbach et al., 2008; Rottman et al., 2012). In Fig. 5A, the biofilm appears bright and the bulk water dark gray due to the differences in their spin relaxation time T_1 (no $scFe_3O_4$-NP addition). The carrier material appears completely black as no signal is exhibited. By the sorption of $scFe_3O_4$-NP to the biofilm, the biofilm becomes darker as the surrounding bulk water (Fig. 5B and C). $scFe_3O_4$-NP serve as contrast agents enabling their visualization with MRI. Consequently, the image contrast is enhanced. $scFe_3O_4$-NP mainly attached to the surface and outer layers of the biofilm. The biofilm is not fully penetrated by $scFe_3O_4$-NP as wrongly suggested by the stereoscopic images. It seems that $scFe_3O_4$-NP were captured by the fluffy structures of the biofilm surface and that there was a transport limitation over the biofilm depth. This supports the assumption that EPS might have collapsed after the exposure of $scFe_3O_4$-NP contributing to the detachment of $scFe_3O_4$-NP loaded biofilm from the carrier material. Using electron microscopy, it has recently been shown that silica-NP and ZnO-NP can be structurally embedded and sorbed to the biofilm surface without necessarily disrupting the cell membranes (Hou et al., 2014; Sibag et al., 2015). This is a sound explanation why the removal of COD during the MBBR experiment remained constant and no measurable inhibition of the microbial activity took place (see Fig. SI 3 in Supporting information). The exposure to 350 mg/L Fe visibly led to a higher biosorption in comparison to 90 mg/L Fe, as the dark regions in the biofilm representing $scFe_3O_4$-NP expanded. This is in accordance with the mass balance of the flow cell experiments (Fig. 2) which proofed that there was a positive correlation between the exposure concentration of $scFe_3O_4$-NP and the degree of biosorption. These results contribute to a better understanding of the fate of $scFe_3O_4$-NP in MBBR systems with heterotrophic biofilms and give indications about the removal mechanisms of $scFe_3O_4$-NP.

4. Conclusions

Knowledge on the interactions between ENP and biofilms is necessary in order to understand the mobility, biosorption and mass flows of ENP in natural as well as in technical environments. This work provides the first evidence about the fate of $scFe_3O_4$-NP in heterotrophic biofilms in flow through systems (flow cell, MBBR). Detailed mass balances for $scFe_3O_4$-NP showed that the biosorption onto heterotrophic biofilms was low, however, it occurred quickly and concentration dependent. The attachment mainly occurred at the outer biofilm layers, which detached after 3 h of exposure in the MBBR. Transport of $scFe_3O_4$-NP in the bulk liquid was more dominant than biosorption, highlighting that the contact time is of subordinated relevance. Most

of the input scFe$_3$O$_4$-NP were stabilized by particulate and dissolved organic matter and were washed out of the systems. This stresses the low retention capacity and the need for strategies to control the release of scFe$_3$O$_4$-NP from biofilm systems, especially in WWT. Further research into bioreactors using various biofilms as well as nanoparticle sorption models would help to better predict the removal of various ENP in biofilm systems, such as MBBR. Furthermore, the impact of different types of ENP on the biological activity in heterotrophic biofilms should be addressed in future experiments.

Acknowledgment

The authors thank Florian Ranzinger for his help with MRI data processing and Reinhard Sembritzki for the ICP-OES measurements. We also thank Laure Cuny for proofreading the manuscript. The authors gratefully acknowledge the German Carl-Zeiss Foundation (PhD Scholarship to M.P. Herrling) and the German Research Foundation (DFG) for their financial support (Instrumental Facility Pro^{2}NMR) and project funding (DE 1839/1-1).

Appendix A. Supplementary data

Supplementary data to this article can be found online at http://dx.doi.org/10.1016/j.scitotenv.2015.11.174.

References

Battin, T.J., Kammer, F.V.D., Weilhartner, A., Ottofuelling, S., Hofmann, T., 2009. Nanostructured TiO_2: transport behavior and effects on aquatic microbial communities under environmental conditions. Environ. Sci. Technol. 43, 8098–8104.

Brar, S.K., Verma, M., Tyagi, R.D., Surampalli, R.Y., 2010. Engineered nanoparticles in wastewater and wastewater sludge — evidence and impacts. Waste Manag. 30, 504–520.

Callaghan, P., 1991. Principles of Nuclear Magnetic Resonance Microscopy. Oxford University Press.

Cuny, L., Herrling, M.P., Guthausen, G., Horn, H., Delay, M., 2015. Magnetic resonance imaging reveals detailed spatial and temporal distribution of iron-based nanoparticles transported through water-saturated porous media. J. Contam. Hydrol. 182, 51–62.

Delay, M., Frimmel, F.H., 2012. Nanoparticles in aquatic systems. Anal. Bioanal. Chem. 402, 583–592.

Delay, M., Dolt, T., Woellhaf, A., Sembritzki, R., Frimmel, F.H., 2011. Interactions and stability of silver nanoparticles in the aqueous phase: influence of natural organic matter (NOM) and ionic strength. J. Chromatogr. A 1218, 4206–4212.

Fabrega, J., Renshaw, J.C., Lead, J.R., 2009. Interactions of silver nanoparticles with *Pseudomonas putida* biofilms. Environ. Sci. Technol. 43, 9004–9009.

Fabrega, J., Zhang, R., Renshaw, J.C., Liu, W.-T., Lead, J.R., 2011. Impact of silver nanoparticles on natural marine biofilm bacteria. Chemosphere 85, 961–966.

Gartiser, S., Flach, F., Nickel, C., Stintz, M., Damme, S., Schaeffer, A., et al., 2014. Behavior of nanoscale titanium dioxide in laboratory wastewater treatment plants according to OECD 303 A. Chemosphere 104, 197–204.

Gottschalk, F., Nowack, B., 2011. The release of engineered nanomaterials to the environment. J. Environ. Monit. 13, 1145–1155.

Gottschalk, F., Kost, E., Nowack, B., 2013a. Engineered nanomaterials in water and soils: a risk quantification based on probabilistic exposure and effect modeling. Environ. Toxicol. Chem. 32, 1278–1287.

Gottschalk, F., Sun, T.Y., Nowack, B., 2013b. Environmental concentrations of engineered nanomaterials: review of modeling and analytical studies. Environ. Pollut. 181, 287–300.

Gu, L., Li, Q., Quan, X., Cen, Y., Jiang, X., 2014. Comparison of nanosilver removal by flocculent and granular sludge and short- and long-term inhibition impacts. Water Res. 58, 62–70.

Herrling, M.P., Fetsch, K.L., Delay, M., Blauert, F., Wagner, M., Franzreb, M., et al., 2015a. Low biosorption of PVA coated engineered magnetic nanoparticles in granular sludge assessed by magnetic susceptibility. Sci. Total Environ. 537, 43–50.

Herrling, M.P., Guthausen, G., Wagner, M., Lackner, S., Horn, H., 2015b. Determining the flow regime in a biofilm carrier by means of magnetic resonance imaging. Biotechnol. Bioeng. 112, 1023–1032.

Hou, L.L., Xia, J., Li, K.Y., Chen, J., Wu, X.L., Li, X.Q., 2013. Removal of ZnO nanoparticles in simulated wastewater treatment processes and its effects on COD and NH^{4+}-N reduction. Water Sci. Technol. 67, 254–260.

Hou, J., Miao, L.Z., Wang, C., Wang, P.F., Ao, Y.H., Qian, J., et al., 2014. Inhibitory effects of ZnO nanoparticles on aerobic wastewater biofilms from oxygen concentration profiles determined by microelectrodes. J. Hazard. Mater. 276, 164–170.

Ikuma, K., Decho, A.W., Lau, B.L.T., 2015. When nanoparticles meet biofilms—interactions guiding the environmental fate and accumulation of nanoparticles. Front. Microbiol. 6.

Jing, H., Mezgebe, B., Aly Hassan, A., Sahle-Demessie, E., Sorial, G.A., Bennett-Stamper, C., 2014. Experimental and modeling studies of sorption of ceria nanoparticle on microbial biofilms. Bioresour. Technol. 161, 109–117.

Kaegi, R., Voegelin, A., Sinnet, B., Zuleeg, S., Hagendorfer, H., Burkhardt, M., et al., 2011. Behavior of metallic silver nanoparticles in a pilot wastewater treatment plant. Environ. Sci. Technol. 45, 3902–3908.

Kaegi, R., Voegelin, A., Ort, C., Sinnet, B., Thalmann, B., Krismer, J., et al., 2013. Fate and transformation of silver nanoparticles in urban wastewater systems. Water Res. 47, 3866–3877.

Kimmich, R., 1997. NMR — Tomography, Diffusometry, Relaxometry. Springer Verlag.

Kiser, M.A., Westerhoff, P., Benn, T., Wang, Y., Perez-Rivera, J., Hristovski, K., 2009. Titanium nanomaterial removal and release from wastewater treatment plants. Environ. Sci. Technol. 43, 6757–6763.

Kiser, M.A., Ryu, H., Jang, H.Y., Hristovski, K., Westerhoff, P., 2010. Biosorption of nanoparticles to heterotrophic wastewater biomass. Water Res. 44, 4105–4114.

Klaine, S.J., Alvarez, P.J.J., Batley, G.E., Fernandes, T.F., Handy, R.D., Lyon, D.Y., et al., 2008. Nanomaterials in the environment: behavior, fate, bioavailability, and effects. Environ. Toxicol. Chem. 27, 1825–1851.

Li, L., Hartmann, G., Döblinger, M., Schuster, M., 2013. Quantification of nanoscale silver particles removal and release from municipal wastewater treatment plants in Germany. Environ. Sci. Technol. 47, 7317–7323.

Limbach, L.K., Bereiter, R., Mueller, E., Krebs, R., Gaelli, R., Stark, W.J., 2008. Removal of oxide nanoparticles in a model wastewater treatment plant: influence of agglomeration and surfactants on clearing efficiency. Environ. Sci. Technol. 42, 5828–5833.

Lowry, G.V., Gregory, K.B., Apte, S.C., Lead, J.R., 2012. Transformations of nanomaterials in the environment. Environ. Sci. Technol. 46, 6893–6899.

Ma, J.Y., Quan, X.C., Si, X.R., Wu, Y.C., 2013. Responses of anaerobic granule and flocculent sludge to ceria nanoparticles and toxic mechanisms. Bioresour. Technol. 149, 346–352.

McQuarrie, J.P., Boltz, J.P., 2011. Moving bed biofilm reactor technology: process applications, design, and performance. Water Environ. Res. 83, 560–575.

Nirschl, H., 2014. Upscaling of Bio-nano-processes: Selective Bioseparation by Magnetic Particles. Springer, Heidelberg, Berlin.

Odegaard, H., Rusten, B., Westrum, T., 1994. A new moving-bed biofilm reactor — applications and results. Water Sci. Technol. 29, 157–165.

Peulen, T.O., Wilkinson, K.J., 2011. Diffusion of nanoparticles in a biofilm. Environ. Sci. Technol. 45, 3367–3373.

Rottman, J., Shadman, F., Sierra-Alvarez, R., 2012. Interactions of inorganic oxide nanoparticles with sewage biosolids. Water Sci. Technol. 66, 1821–1827.

Schaumann, G.E., Philippe, A., Bundschuh, M., Metreveli, G., Klitzke, S., Rakcheev, D., et al., 2015. Understanding the fate and biological effects of Ag- and TiO_2-nanoparticles in the environment: the quest for advanced analytics and interdisciplinary concepts. Sci. Total Environ. 535, 3–19.

Sibag, M., Choi, B.-G., Suh, C., Lee, K.H., Lee, J.W., Maeng, S.K., et al., 2015. Inhibition of total oxygen uptake by silica nanoparticles in activated sludge. J. Hazard. Mater. 283, 841–846.

Sun, T.Y., Gottschalk, F., Hungerbuehler, K., Nowack, B., 2014. Comprehensive probabilistic modelling of environmental emissions of engineered nanomaterials. Environ. Pollut. 185, 69–76.

Tan, M., Qiu, G., Ting, Y.-P., 2015. Effects of ZnO nanoparticles on wastewater treatment and their removal behavior in a membrane bioreactor. Bioresour. Technol. 185, 125–133.

Wang, Y., Westerhoff, P., Hristovski, K.D., 2012. Fate and biological effects of silver, titanium dioxide, and C-60 (fullerene) nanomaterials during simulated wastewater treatment processes. J. Hazard. Mater. 201, 16–22.

Wessman, F.G., Yuegen, E.Y., Zheng, Q., He, G., Welander, T., Rusten, B., 2004. Increasing the capacity for treatment of chemical plant wastewater by replacing existing suspended carrier media with Kaldnes Moving Bed™ media at a plant in Singapore. Water Sci. Technol. 49, 199–205.

Westerhoff, P.K., Kiser, A., Hristovski, K., 2013. Nanomaterial removal and transformation during biological wastewater treatment. Environ. Eng. Sci. 30, 109–117.

Yang, Y., Wang, Y., Hristovski, K., Westerhoff, P., 2015. Simultaneous removal of nanosilver and fullerene in sequencing batch reactors for biological wastewater treatment. Chemosphere 125, 115–121.

Yuan, Z.-H., Yang, X., Hu, A., Yu, C.-P., 2015. Long-term impacts of silver nanoparticles in an anaerobic–anoxic–oxic membrane bioreactor system. Chem. Eng. J. 276, 83–90.

Zhang, Y., Chen, Y.S., Westerhoff, P., Crittenden, J., 2009. Impact of natural organic matter and divalent cations on the stability of aqueous nanoparticles. Water Res. 43, 4249–4257.